Reprinted from JOURNAL OF PHYSICAL OCEANOGRAPHY, Vol. 21, No. 12, December 1991
American Meteorological Society

The Seasonal Cycle of Wind-Stress Curl in Subtropical Eastern Boundary Current Regions

ANDREW BAKUN AND CRAIG S. NELSON*

Pacific Fisheries Environmental Group, Southwest Fisheries Science Center, NOAA/NMFS, Monterey, California

(Manuscript received 2 April 1990, in final form 29 April 1991)

ABSTRACT

Historical surface marine wind reports have been processed to define characteristic seasonal distributions of wind-stress curl over the four major eastern boundary current regions of the World Ocean (i.e., the California, Canary, Benguela, and Peru/Humboldt systems) on smaller scales than previously available. Interregional comparisons show that these "classical" coastal upwelling systems are characterized by cyclonic wind-stress curl near the continental boundaries and anticyclonic curl offshore, in association with predominantly equatorward (upwelling favorable) alongshore wind stress. The cross-shore profile of alongshore stress typically has an offshore maximum located some 200 to 300 km from the coast. The decay of the wind stress toward the coast defines a region of cyclonic wind-stress curl, where coastal upwelling is enhanced by curl-induced oceanic upwelling (Ekman pumping). During summer in the respective hemispheres, the region of cyclonic curl expands poleward in each boundary current system. Particularly intense cyclonic curl occurs adjacent to capes during summer coastal upwelling maxima. During fall and winter when the upwelling system weakens, the latitudinal extent of cyclonic curl adjacent to the coast contracts, and the most intense cyclonic curl is usually associated with coastal bights.

1. Introduction

The curl of the wind stress acting on the sea surface is a fundamental forcing agent for dynamic ocean processes. It stands out as the external input term in ocean model formulations expressed in terms of vorticity balance. The same process, when considered from the viewpoint of vertical structure in the flow field, appears as the divergence of surface Ekman transport. Wind-stress curl thus controls "Ekman pumping" and associated vertical advection in regions seaward of the immediate effects of coastal boundaries (Yoshida 1955a; Yoshida and Mao 1957; Smith 1968) and so may have a variety of physical, chemical, and biological consequences to the ocean ecosystem. Potential mechanisms include rearrangements of the mass field and corresponding changes in the current structure (Yoshida 1955b), generation of baroclinic Rossby waves (White 1985; Cummins et al. 1986), and other significant contributions to variability in the coastal ocean on shorter space and time scales (Carton and Philander 1984; Brink et al. 1987; Rienecker et al. 1987). In addition, various models of eastern ocean boundary current dynamics (e.g., Hurlburt and Thompson 1973; Pedlosky 1974; McCreary et al. 1987) feature cyclonic wind-stress curl near the coast as a contributing factor for poleward undercurrents, and a suggestive correspondence between cyclonic wind-stress curl near the coast in the California Current System and the presence of eastern boundary poleward coastal counterflows has been pointed out (Munk 1950; Nelson 1977; Hickey 1979). In addition to such dynamical effects, the vertical transfers of physical and chemical properties associated with Ekman pumping can also have major effects on the biological system (Chelton 1982; Peláez and McGowan 1986; Abbott and Zion 1987).

No actual measurements of wind-stress curl are available except in rare instances where arrays of research ships or buoys have been used to make coordinated wind measurements (e.g., Halpern 1976; Düing et al. 1980) or when scatterometer data have been analyzed to construct wind-stress fields (e.g., Perigaud et al. 1989). Synoptic samplings of maritime reports may adequately define very large-scale variations (e.g., thousands of kilometers) in the wind-stress curl patterns (Willebrand 1978; Chelton 1980), but not the intermediate scales (tens to hundreds of kilometers) on which important ocean responses and biological effects are expected to occur.

Early descriptions of wind-stress curl over the ocean focused on ocean basin scales. Saunders (1976) demonstrated the effects of grid size on calculations of wind-

* Present affiliation: Department of Oceanography, Naval Postgraduate School and Office of Ocean and Earth Sciences, NOAA/NOS.

Corresponding author address: Dr. Andrew Bakun, Pacific Fisheries Environmental Group, Southwest Fisheries Science Center, NOAA/NMFS, P.O. Box 831, Monterey, CA 93942.

stress curl and suggested that large-scale calculations underestimate the curl magnitude. Efforts to resolve mesoscale details either have involved improvements in grid resolution (Wyrtki and Meyers 1976; Hastenrath and Lamb 1977; Goldenberg and O'Brien 1981; Hellerman and Rosenstein 1983; Rienecker and Ehret 1988) or have relied on smooth curvilinear interpolations of the larger scale (Roden 1972; Evenson and Veronis 1975).

The finest-scale distributions of wind-stress curl that have been published are Nelson's (1977) mean monthly charts for the California Current region. Nelson's computational grid contains intersections at 1° latitude/longitude intervals, each intersection being the center of a 1° × 1° square area. His curl calculation employs central difference derivatives that span three grid intersections in both the zonal and meridional directions, thereby incorporating data over spans of 3° of both latitude and longitude for each computed value of the curl. The distance scale for the derivative is fixed at 2° latitude or longitude (Fig. 1a).

In this study, we further refine the scale of the curl computation (1° rather than 2° scale for the finite-difference derivatives) for the California Current System and also expand coverage to the three other "classical" subtropical eastern boundary current systems (Wooster and Reid 1963): the Canary, Benguela, and Peru/Humboldt Current systems (Fig. 2). An additional first-order correction for nonuniform distribution of reports within a given 1° × 1° square summary area is also added by adjusting for the differences between the mean latitude and longitude of the reports and the geographic center of the summary area. This avoids the possibility of grossly erroneous wind-stress curl magnitudes in cases where reports may be concentrated along narrow shipping lanes, which may not cross near the center of the 1° × 1° square.

To produce these distributions, maritime data from a large number of years are composited together to yield mean wind-stress patterns on much finer scales than are definable in synoptic samples of these data.

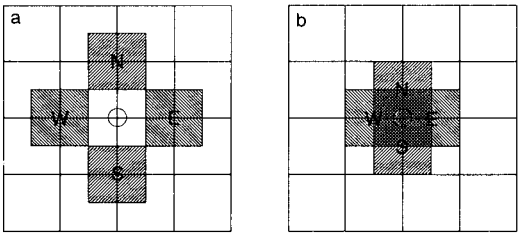

FIG. 1. Computational grids used for wind-stress curl calculations. Grid intersections are spaced 1° latitude by 1° longitude apart. (a) The central difference scheme of Nelson (1977) yields a 2° length scale for the derivatives. (b) The staggered grid used in this study in which 1° × 1° summary areas for the separate wind-stress components overlap allows a 1° length scale for the finite-difference computations.

Interannual variability is suppressed by compositing many years together, revealing characteristic seasonalities. As shown below, the curl is a linear mathematical operator and therefore the field of curl of the mean wind stress will, as sampling error decreases, tend increasingly to resemble the true mean field of the curl of the wind stress.

These higher resolution distributions are intended to serve as checks for possible scale-related artifacts in Nelson's (1977) results for the California Current region. Corresponding distributions for the eastern boundary current regions of the North and South Atlantic oceans, and of the South Pacific Ocean, are intended to provide indications of the generality of the various features and to constitute a basis for applying the "comparative method" (e.g., Bakun and Parrish 1990) to classify and interpret similar characteristics in the wind-stress curl patterns among the four regions, and to draw conclusions as to their dynamical and ecological significances.

2. Methods

a. Data processing and computation procedures

Ship wind reports were extracted from the NOAA National Climatic Data Center's (NCDC) global file of surface marine observations (Tape Data Family-11). A single-pass editor was used to ensure physically possible values and to remove other gross errors in the data, including obviously erroneous position reports and wind observations exceeding extreme magnitude limits.

The stress estimates are computed from individual wind reports according to the bulk aerodynamic formula

$$\boldsymbol{\tau} = \rho C_d |\mathbf{V}| \mathbf{V}, \tag{1}$$

where $\boldsymbol{\tau}$ is the stress vector, ρ is the density of air, C_d is a dimensionless drag coefficient, $\mathbf{V}$ is the wind velocity, and $|\mathbf{V}|$ is the wind speed. Following Nelson (1977), the parameters C_d and ρ are held constant (0.0013 and 0.00122 g cm^{-3}).

Summary grids of one-degree latitude/longitude areal quadrangles were set along the mainly meridional portions of the continental boundaries of the four regions (Fig. 2), so as to cover the generally equatorward eastern boundary current flows and the associated temperate coastal upwelling systems. In each region the summary grid roughly parallels the coastline configuration and extends from the coast to between 11° and 15° longitude offshore. The scale of the curl computation is minimized, while maintaining a 1° × 1° areal sample size for each mean stress component estimate by employing a "staggered" grid arrangement in which the grids for the respective zonal and meridional wind stress component summaries are offset from one another by 0.5° in both latitude and longitude

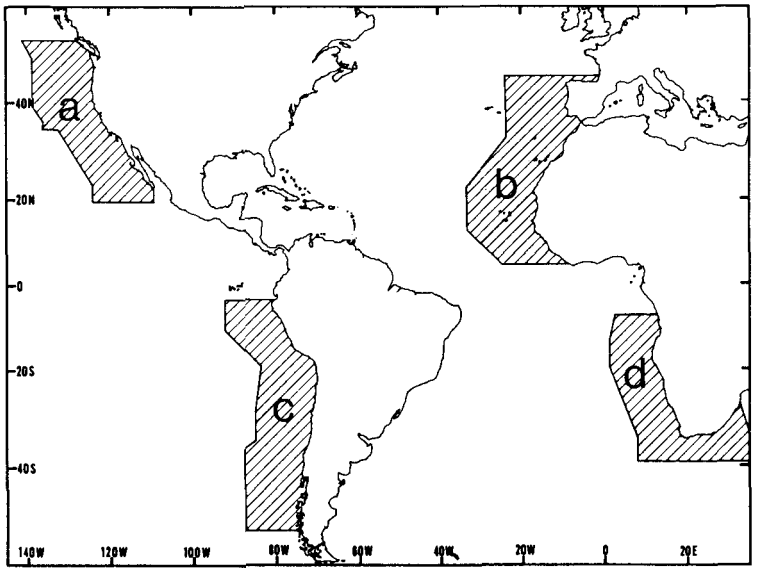

FIG. 2. Subtropical eastern boundary current domains for which wind-stress curl distributions are mapped in Figs. 7–10. (a) California Current region, (b) Canary Current region, (c), Peru/Humboldt Current region, and (d) Benguela Current region.

(Fig. 1b). Long-term composite seasonal distributions were constructed by averaging all available data within each 1° × 1° square over each of six 2-month segments of the annual cycle.

Available data density is highly variable among regions and within regions (Fig. 3). The version of the data file used contains data extending from the nineteenth century through 1979. Total numbers of observations range from fewer than 0.3 million reports in the Peru/Humboldt Current region to more than 3.3 million reports for the Canary Current system. Individual 1° × 1° areal samples contain less than 50 observations for the entire period in some regions off Peru and Chile, but in excess of 40 000 observations in portions of the Southern California Bight and off the Iberian Peninsula. The highest density of reports lies within 300 km of each coast, along the primary shipping routes, except off southwestern Africa, where the narrow, transoceanic shipping lane diverges from the coast (Fig. 3d).

Prior to 1950, a large percentage of the available maritime reports contain positions reported only to the nearest whole degree of latitude and longitude. These reports are not amenable to the staggered grid computation scheme in which the samples of the respective wind-stress components are offset by 0.5° in each coordinate direction. Accordingly, the 30-year period, 1950–79, has been chosen as the basic time frame for compositing data to construct the wind stress and wind-stress curl fields. One deviation from this procedure was required to construct the distributions for the Peru/Humboldt Current region where data density is an order of magnitude lower than the other three regions (Fig. 3). Because of the extremely undersampled nature of the distributions, it was deemed necessary to relax our procedures somewhat for much of the Peru/Humboldt Current region to incorporate all the available data in the historical record (1850–1979). For the major portion of that particular region, older data with positions that may have been reported only to whole degrees of latitude and longitude were treated as if they were actually accurately positioned at the integral 1° latitude/longitude intersections. Each of the 2-month, seasonal wind-stress curl distributions for the Peru/Humboldt Current region is based on approximately one-sixth of the total available data density depicted in Fig. 3c. For the California, Canary, and Benguela current systems, the data density reflected in these computations is reduced by an additional factor of approximately one-half because only data since 1950 have been used for these three regions.

In spherical coordinates, the vertical component of the curl of the wind stress on the sea surface, $\mathbf{k} \cdot \nabla \times \tau$, is calculated as

$$\mathbf{k} \cdot \nabla \times \tau = \frac{1}{R \cos\phi} \left[\frac{\partial \tau_\phi}{\partial \lambda} - \frac{\partial (\tau_\lambda \cos\phi)}{\partial \phi} \right], \quad (2)$$

where R is the mean radius of the earth, ϕ and λ are the latitude and longitude (in radians), and $\partial \tau_\phi / \partial \lambda$ and $\partial (\tau_\lambda \cos\phi)/\partial \phi$ are the zonal derivative of merid-

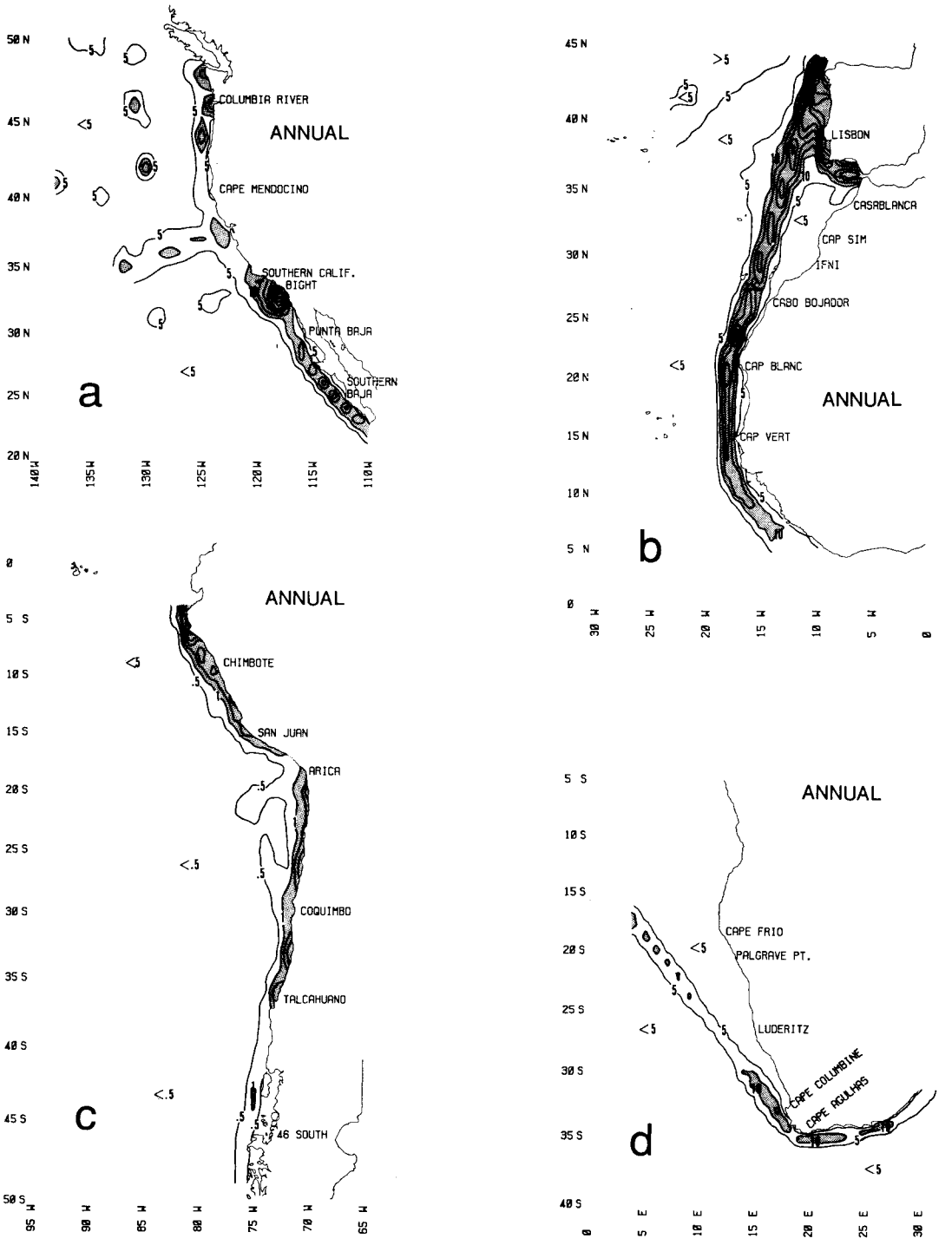

FIG. 3. Distribution of observations ($\times 10^3$) per $1° \times 1°$ quadrangle in the four eastern boundary current regions for the period extending from the late nineteenth century through 1979. (a) California Current region, (b) Canary Current region, (c) Peru/Humboldt Current region, and (d) Benguela Current region. Contour interval is 5000 and values greater than 10 000 observations per $1° \times 1°$ box are shaded in (a), (b), and (d). Contour interval is 500 and values greater than 1000 observations per $1° \times 1°$ box are shaded in (c).

ional stress and the meridional derivative of zonal stress, respectively.

The finite difference form of (2) is

$$\mathbf{k}\cdot\nabla\times\tau = \frac{1}{R\cos\phi}\left[\frac{\tau_{\phi(E)}-\tau_{\phi(W)}}{\Delta\lambda} - \frac{\tau_{\lambda(N)}\cos\phi(N)-\tau_{\lambda(S)}\cos\phi(S)}{\Delta\phi}\right], \quad (3)$$

where $\tau_{\phi(E)}$, $\tau_{\phi(W)}$, $\tau_{\lambda(N)}$, and $\tau_{\lambda(S)}$ are the averages of the wind-stress component estimates in the four 1° × 1° summary areas involved in a given calculation (Fig. 1b), and $\Delta\lambda$ and $\Delta\phi$ are the differences in the mean longitudes in the two areal segments involved in the zonal derivative and the mean latitudes in the two areal segments involved in the meridional derivative, respectively.

To estimate sampling error, the characteristic long-term seasonal wind stress distributions are considered to be sufficiently well sampled for the standard error of the mean to provide a reasonable estimate of error. Accordingly, the variances of the 1° × 1° stress component samples are carried through the curl calculation following standard procedures (Beers 1953), that is,

$$\sigma^2_{\text{curl}} = \frac{1}{R\cos\phi}\left[\frac{\sigma^2_{\tau_{\phi(E)}}+\sigma^2_{\tau_{\phi(W)}}}{\Delta\lambda} + \frac{\cos^2\phi(N)\,\sigma^2_{\tau_{\lambda(N)}}+\cos^2\phi(S)\,\sigma^2_{\tau_{\lambda(S)}}}{\Delta\phi}\right], \quad (4)$$

where σ^2_{curl} represents the variance of the curl estimate, and $\sigma^2_{\tau_{\phi(E)}}$, $\sigma^2_{\tau_{\phi(W)}}$, $\sigma^2_{\tau_{\lambda(N)}}$, and $\sigma^2_{\tau_{\lambda(S)}}$ represent the variances of the estimates of the stress components appearing in (3).

b. Error analysis

Various errors may introduce uncertainties into the quantities appearing in (3). These errors may be classified as being either systematic or random (Weare 1989). Systematic error that might be due to inadequacy of the bulk formulation approach itself is hard to assess (Hsiung 1986). Direct sea surface stress measurements are difficult and there is large scatter in the results. Certainly, systematic direct measurements of wind stress have not been made under all ocean conditions, various proximities to coastal features, and other possible effects that occur within the areas addressed in this study.

The most obvious uncertainty of the systematic type is the use of a constant drag coefficient, C_d, in the stress computation (1). It seems clear that the value of C_d is dependent on both wind speed and atmospheric stability (Large and Pond 1981; Blanc 1985; Smith 1988; Trenberth et al. 1989). However, there is no universally adopted variable formulation for C_d at the present time, and research on the problem is a continuing activity. Because of this, it has become common to avoid this particular issue by computing a quantity called the pseudostress (Goldenberg and O'Brien 1981; Servain and Legler 1986; Breidenbach 1990), which is the stress divided by ρC_d (i.e., a vector with magnitude equal to the wind speed squared and having the same direction as the wind velocity).

One important use of the distributions we have produced will be in applications of the comparative method (Bakun and Parrish 1990) to draw inferences concerning important scales that are not amenable to experiments or directed observational programs. By retaining a constant factor for ρC_d, our results are equivalent to results expressed in terms of pseudostress, but scaled so as to carry actual stress units and to reflect reasonable magnitudes with respect to those units. This particular constant factor serves to make our results directly comparable with results of Nelson (1977), Wooster et al. (1976), Bakun (1978), Parrish et al. (1983), Bakun and Parrish (1990), Bakun (1990), and various other studies that have employed an identical formulation. Similarly, they can be readily made comparable to any of the many other studies using constant coefficient formulations by simple multiplication by an appropriate ratio of the constant factors.

Magnitudes of wind stress computed according to our constant factor formulation and a formulation presented by Large and Pond (1981), which includes wind-speed dependence are compared in Fig. 4. Wind-speed distributions in subtropical eastern ocean boundary regions tend to have a mode near 5–7 m s^{-1} and contain relatively few observations exceeding 14 m s^{-1} (Nelson 1977). In this range, the two formulations (Fig. 4) yield very similar stress estimates. Thus, the constant and wind-speed–dependent drag coefficient formulations should not produce widely differing long-term averages.

With regard to the effect of atmospheric stability, it has been previously demonstrated for similar one-degree summaries in the California Current region (Nelson 1977), and on larger scales for all four regions

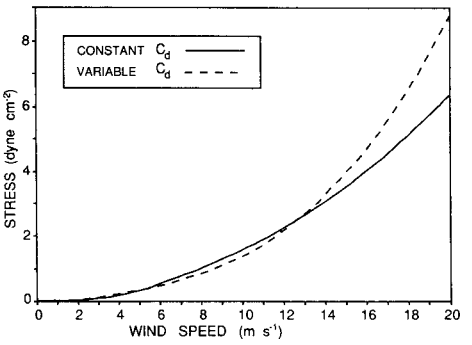

FIG. 4. Comparison of stresses computed with constant and wind-speed-dependent drag coefficient formulations.

(Hellerman and Rosenstein 1983), that the effect of stability on averages of computed stresses in eastern boundary regions is only of the order of several hundredths of a dyn cm^{-2}. There also seems to be little significant spatial pattern in the stability effect that could substantially affect derived wind-stress curl distributions. One exception indicated by Hellerman and Rosenstein (1983) is an area directly off the southern tip of Africa, where neglect of the effect of atmospheric stability may lead to an underestimate of the order of 0.1 dyn cm^{-2}. The bulk of the available wind reports in the pre-1980s historical files are Beaufort estimates rather than anemometer measurements. These estimates, which are based on visual effects of winds on the sea surface, are "raised" to reflect a 10-m "mast height" reference using conversion tables that largely assume a neutral stability profile. In transferring what was originally sea surface information from the 10-m reference height down to the sea surface level at which the stress is determined, it seems appropriate to adhere to the same assumption. In regard to air density, ρ, any effect of a constant value in the stress computation will be small in these regions, where the airflow is generally from the ocean toward the continent and where effects of upwelling and advection tend to damp the seasonal temperature cycle.

The fraction of anemometer measurements in the marine report files has been increasing over recent decades (Ramage 1987). It appears that the majority of ship anemometers are actually installed at greater heights above the sea surface than the 10-m standard height to which the Beaufort estimates and bulk stress formulas are calibrated (Cardone et al. 1990). This would cause an overestimate of the wind at 10 m, which would lead to a corresponding overestimate of the sea surface stress. Thus, there may be an artificial increasing trend in wind speeds inferred from the maritime data files. However, such a trend should not affect the spatial pattern in long-term averages of wind stress and wind-stress curl, unless there were spatial patterns in the trend. Although the proportion of anemometer-based reports appears to have increased more rapidly in the Pacific than in the Atlantic, there is no reason to suspect spatial pattern in the trend within regions.

The Beaufort wind estimates themselves may have systematic errors. The British (e.g., Shearman 1983) apparently prefer the Beaufort estimate over actual wind measurements because the sea state reflects an integration of the wind effects over about an hour, whereas measured winds reflect a much more instantaneous description. However, Böning et al. (1991) indicate that the official World Meteorological Organization (WMO) conversion scale for Beaufort estimates systematically underestimates low wind speeds and overestimates high wind speeds. Isemer and Hasse (1991) demonstrate that the effect on the climatological wind-stress curl distribution could be substantial, resulting in as much as a 30% underestimate of total Sverdrup transport integrated westward across the North Atlantic Ocean from the eastern boundary.

In summary, there are several possible sources of systematic error in the quantities used in the stress computation. Of those for which it is possible to guess a probable tendency for bias, the lack of a wind speed dependence in the drag coefficient would seem to lead, if anything, to an underestimate because of suppression of the effect of particularly high wind speeds, as would the effect of errors in the WMO–Beaufort conversion scale. The effect of anemometer measurements would be toward an overestimate. Because of the nonlinearity in the stress computation (1), quasi-random error variance in the wind observations will itself lead to some degree of systematic overestimate of the average stress (e.g., an error of increased wind speed will make more contribution to the average stress than an equal error of reduced wind speed). Thus, at least some of the different sources of systematic error would seem to counteract one another to some degree.

In any case, on the small scales of these computations, the true long-term mean, spatially adjacent stress vectors must be largely codirectional. Therefore, systematic uncertainties will tend to be in the same sense in adjacent samples and thus to be somewhat self-canceling in the subtractions involved in forming the finite-difference derivatives in (3). They will produce generally equivalent percentage uncertainties in the curl magnitudes to those produced in the stress magnitudes (i.e., perhaps from a few percent to certainly not more than 10 to 20 percent). It is well known that the magnitude of sea surface wind-stress curl is highly scale dependent in any case (e.g., Saunders 1976; Hellerman and Rosenstein 1983). In this study we are interested in spatial pattern in the wind-stress curl field (e.g., the locations of maxima, minima, strong gradients, the "zero-curl contour" where the sea surface Ekman transport field changes from convergent to divergent, etc.). These aspects should not be substantially affected by systematic errors.

A much greater problem than systematic errors (particularly to a study like ours where the focus is on mesoscale pattern rather than on integrated ocean basin-scale effects) is the more random type of error inherent in marine weather reports. These include imprecision and mistakes in the observations, but also errors in recording of the data in logbooks and in the manual extraction and redigitization process. For example, a not uncommon error occurs in coding the correct hemisphere for the geographical position (one can see this in global maps of maritime report positions in which, when a long enough period to assemble sufficient numbers of reports is incorporated, "reflections" of major shipping routes located in an opposite hemisphere may appear to traverse land areas, ocean areas of particularly low report densities, etc.). Clearly, this can be a serious problem where, for example, a few observations taken during the winter season from

heavily sampled areas near the U.S. East Coast, north of Cape Hatteras could erroneously reflect across the equator to appear in an extremely sparsely sampled (Fig. 3) summer situation near the Chilean coast, south of Talcahuano. Likewise, observations from within the Mediterranean Sea might erroneously reflect into data poor offshore regions off southern Africa, and observations near Hong Kong Harbor might reflect across the Greenwich meridian to appear in the data poor areas offshore of southern Baja California.

These errors combine with real natural variability to produce large variances in the wind sample distributions. These are, in turn, amplified in the nonlinear stress calculation (1) and again in the differencing operations involved in the curl computation (3). This results in very "noisy" distributions of one-degree wind-stress curl estimates, carrying large and variable standard error estimates computed according to (4). The wide scatter of standard error estimates in the subsample illustrated in Fig. 5 is typical. Comparisons among differently constituted subsamples indicate some degree of dependence on season, with winter seasons yielding slightly higher average standard errors than summer, and a larger degree of dependence on latitude (for example, "smoothed" values of the standard errors tend to be about 25% less in samples of the latitude band from 9° to 19° than in samples of the band from 23° to 33°). No clear differences between the regions are apparent once the seasonal and latitudinal dependencies have been considered. As might be inferred from the latitudinal and seasonal dependencies, the standard error appears to increase with mean curl magnitude. However, the increase in standard error is slower than the increase in magnitude (Fig. 6). Thus, higher magnitudes of computed curl, while generally carrying greater standard errors, tend to be more significant than low curl magnitudes. However, as expected, both the characteristic mean level of standard error and its scatter decreases with increasing numbers of observations incorporated in the calculation (Fig. 5).

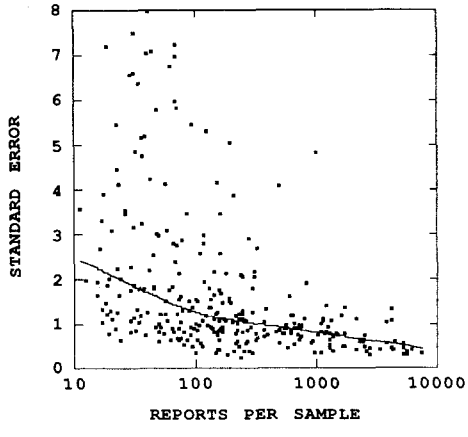

FIG. 5. Typical scatterplot of standard error calculations (1×10^{-8} dyn cm^{-3}) versus average number of observations in the four 1° areal samples used in the curl calculation. The curve was fitted to the data by robust locally weighted regression using the LOWESS method (Cleveland 1981).

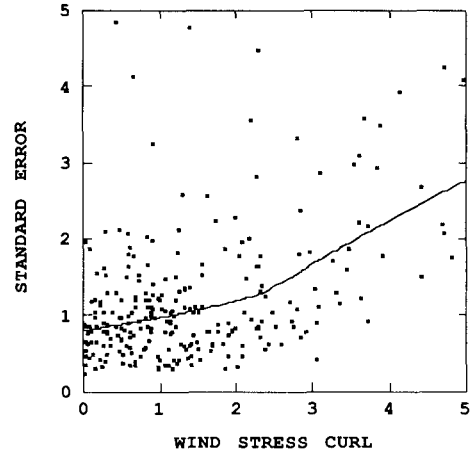

FIG. 6. Typical scatterplot of standard error calculations versus computed wind-stress curl magnitude (1×10^{-8} dyn cm^{-3}). The curve was fitted to the data by robust locally weighted regression using the LOWESS method (Cleveland 1981).

c. *Construction of smoothed curl fields*

In Nelson's (1977) contoured charts for the California Current region, noise was not suppressed, essentially leaving it to the viewer to determine the significant patterns, taking into account the visual indication of the noise component. However, this led to confusion among certain users, who apparently had difficulty in distinguishing real features from sampling error. In the present study, the choice was made to deal with the noise through analysis and smoothing, but to attempt to retain the finest scale of significant pattern available in any location. Of course, this varies greatly both within and among the four regions due to the geographical differences both in available data densities (Fig. 3) and in actual conditions. Accordingly, no smoothing of the stress fields was performed prior to the curl computation. Several steps, which combined both objective and subjective approaches, were taken to deal with the resulting noise component to yield significant, recognizable wind-stress curl patterns.

In addition to the 2-month segments of the seasonal cycles, which form the basic temporal unit of this study (i.e., the presentations in Figs. 7 to 10), separate independent single-month mean distributions of wind stress and wind-stress curl were also prepared and subjected to the same treatments enumerated next. These

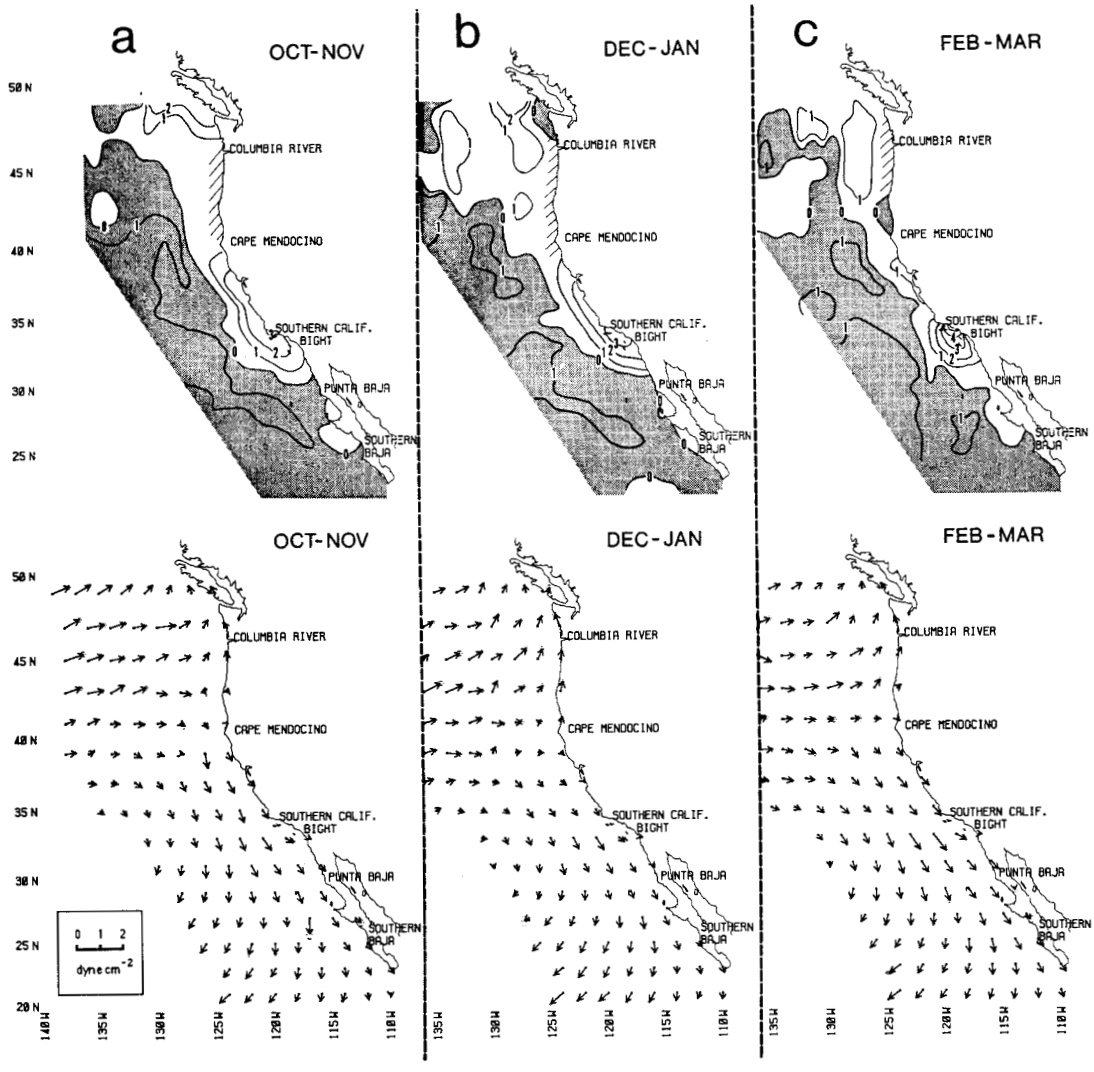

FIG. 7. California Current region: wind-stress curl (10^{-8} dyn cm^{-3}) and surface wind stress (dyn cm^{-2}) distributions. Contour interval is 1×10^{-8} dyn cm^{-3} and regions of anticyclonic curl are shaded. Wind-stress vectors are plotted at alternate latitude and longitude intersections, and symbols are scaled according to the key on the chart. (a) October–November, (b) December–January, (c) February–March,

provided dual independent checks on wind-stress curl features within each of the 2-month seasonal segments for which composite distributions are presented. Preliminary objectively contoured maps of all the 1-month and 2-month distributions, in their original state, were prepared as a first step in the process of constructing characteristic distributions.

Companion maps of discrete symbols indicating both magnitude and standard error for each gridpoint estimate of wind-stress curl were also prepared for all the 1-month and 2-month distributions. These provided a readily referenced estimate of the reliability of each computed wind-stress curl value. Another guide to significance was provided by the degree of spatial and temporal coherence among the independent estimates (except in locations directly adjacent to prominent coastal features where spatial coherence might not be expected). That is, features that were coherently indicated on scales larger than $2° \times 2°$ squares (because directly adjacent one-degree curl estimates share data and, so, are not independent) and in both single-month subsamples of a 2-month set were assigned high prob-

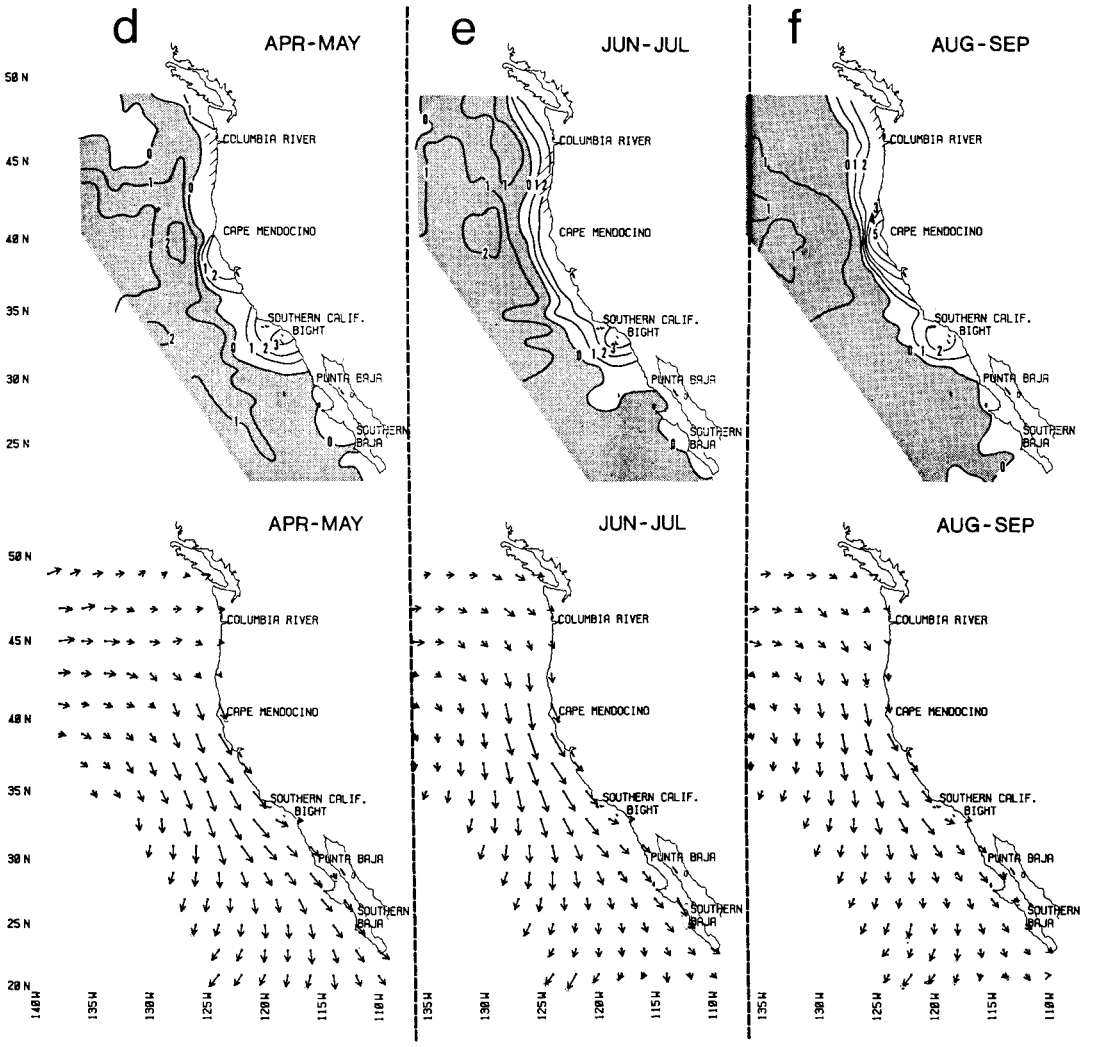

FIG. 7. (*Continued*) (d) April–May, (e) June–July, and (f) August–September.

ability of reality. The intent was to be conservative in the subjective mapping process and to avoid defining questionable features.

Maps of spatially smoothed, 2-month wind-stress curl distributions were also prepared and objectively contoured. A nonlinear smoother was employed. The usual linear smoothing techniques were deemed inadequate in this case, as they merely spread intense bull's-eyes, which largely obscured the underlying significant patterns in the data-poor areas. Rather, a 3 × 3 gridpoint version of the nonlinear median smoother (Beaton and Tukey 1974; Rabiner et al. 1975) was employed, whereby the value at each grid location was replaced by the median of the nine values in the 3 × 3 grid segment centered at the location. The grid indexing was set up such that the zonal grid coordinate was referenced to the coastline rather than to a constant longitude. Where the coastline trend deviated from a largely meridional orientation, the 3 × 3 filter "rectangle" was distorted into somewhat of a "parallelogram" shape, with the sloping sides of the parallelogram oriented generally along the trend of the coast.

These objectively filtered maps provided a fairly smoothed, organized background. However, details that may have been lost in the filtering process, but

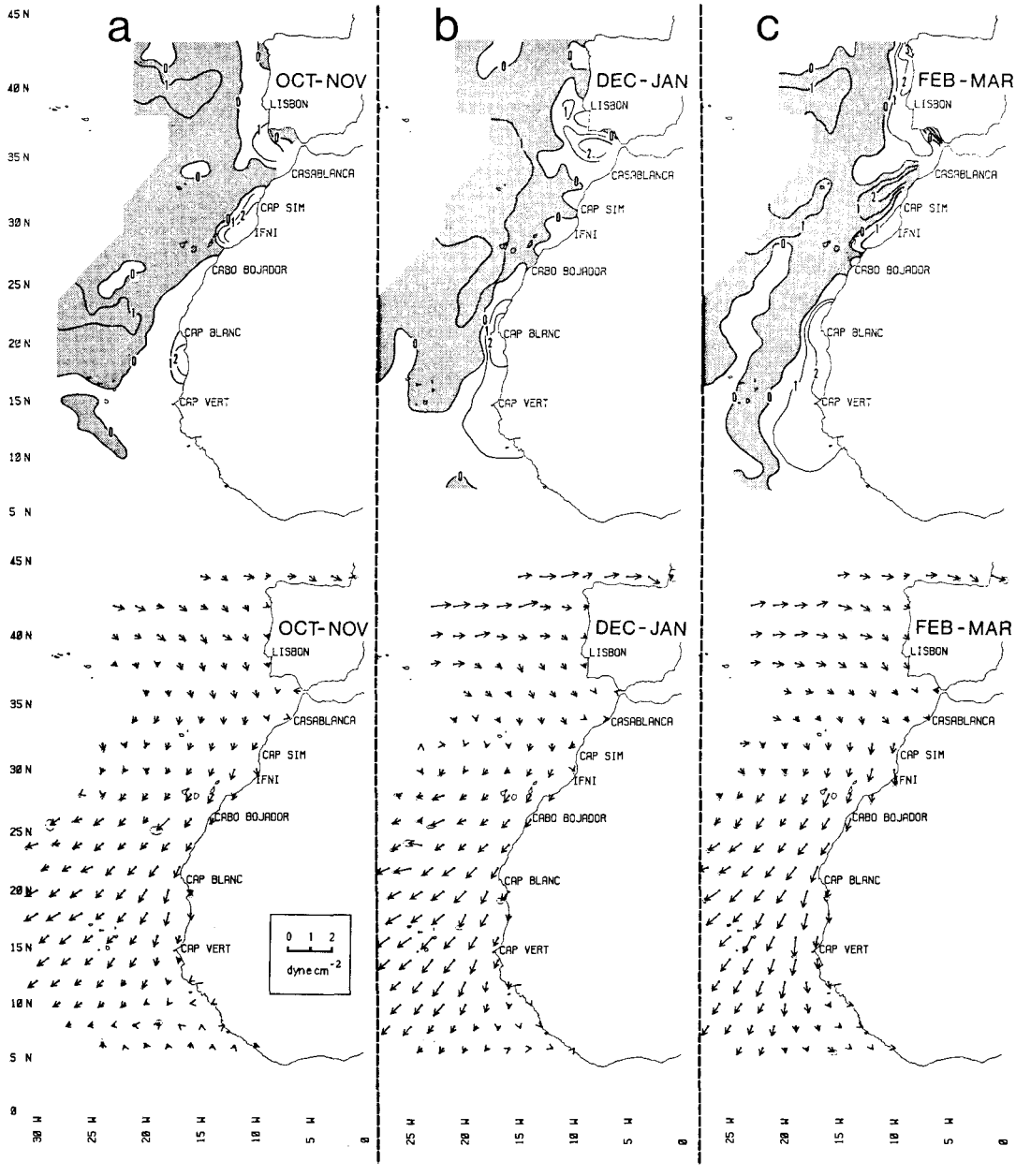

FIG. 8. Canary Current region: wind-stress curl (10^{-8} dyn cm^{-3}) and surface wind-stress (dyn cm^{-2}) distributions. Contour interval is 1 $\times 10^{-8}$ dyn cm^{-3} and regions of anticyclonic curl are shaded. Wind-stress vectors are plotted at alternate latitude and longitude intersections, and symbols are scaled according to the key on the chart. (a) October–November, (b) December–January, (c) February–March,

were indicated as significant by the other aforementioned examinations were added by overlaying the smoothed and unsmoothed distributions and drawing the final contours, while continually referring to the 1-month subsample distributions and to the maps of discrete symbols carrying the standard error indicators as

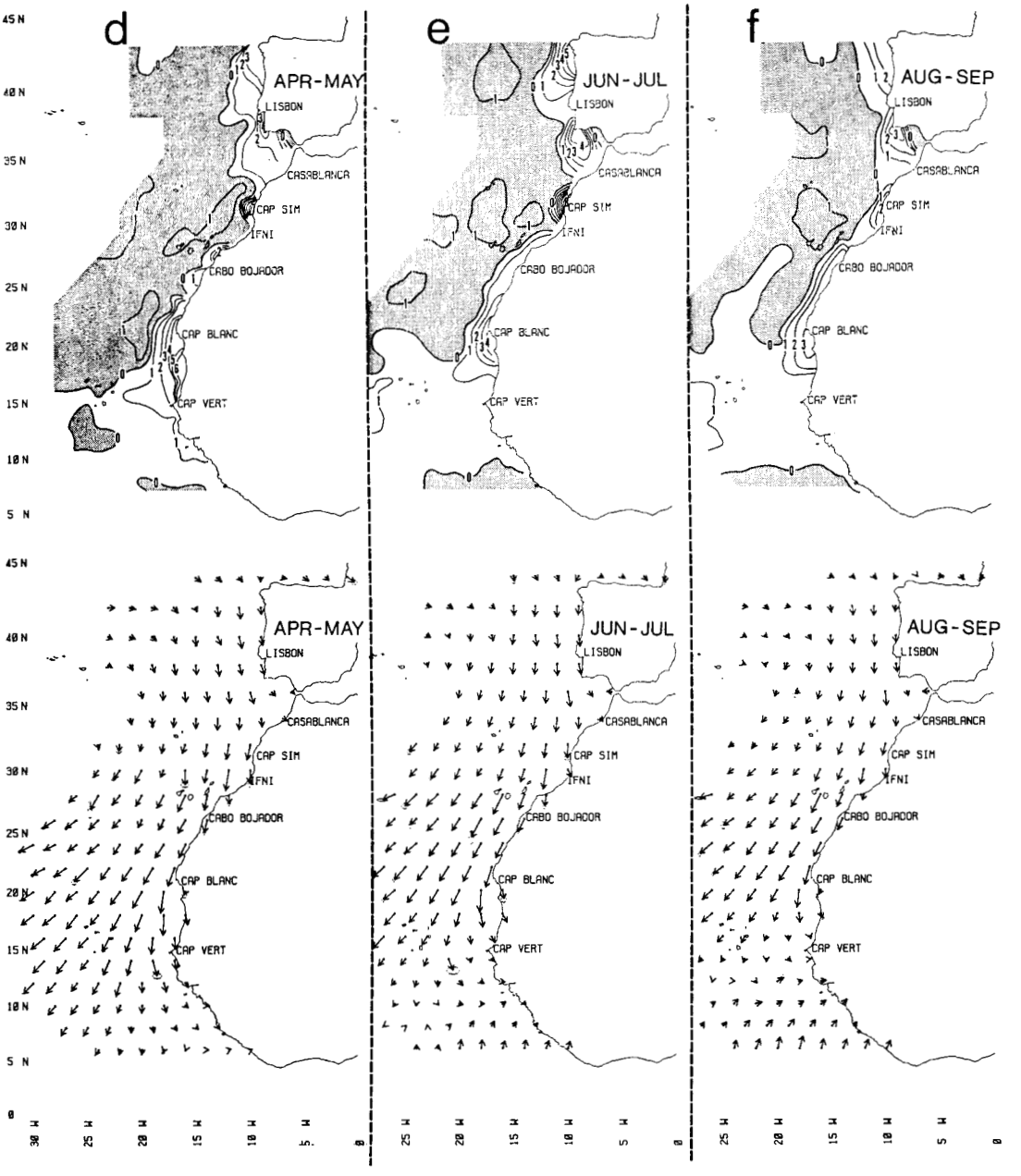

FIG. 8. (*Continued*) (d) April–May, (e) June–July, and (f) August–September.

guides. This subjective process was necessary to extract the maximum amount of information supported by the data. The largest sampling errors were often due to a "data problem" in a particular one-degree areal sample. Because each sample contributes to two adjacent curl computations, the effect is reflected as two adjacent anomalous "spikes" of opposite sign, each carrying a very large standard error estimate. It was

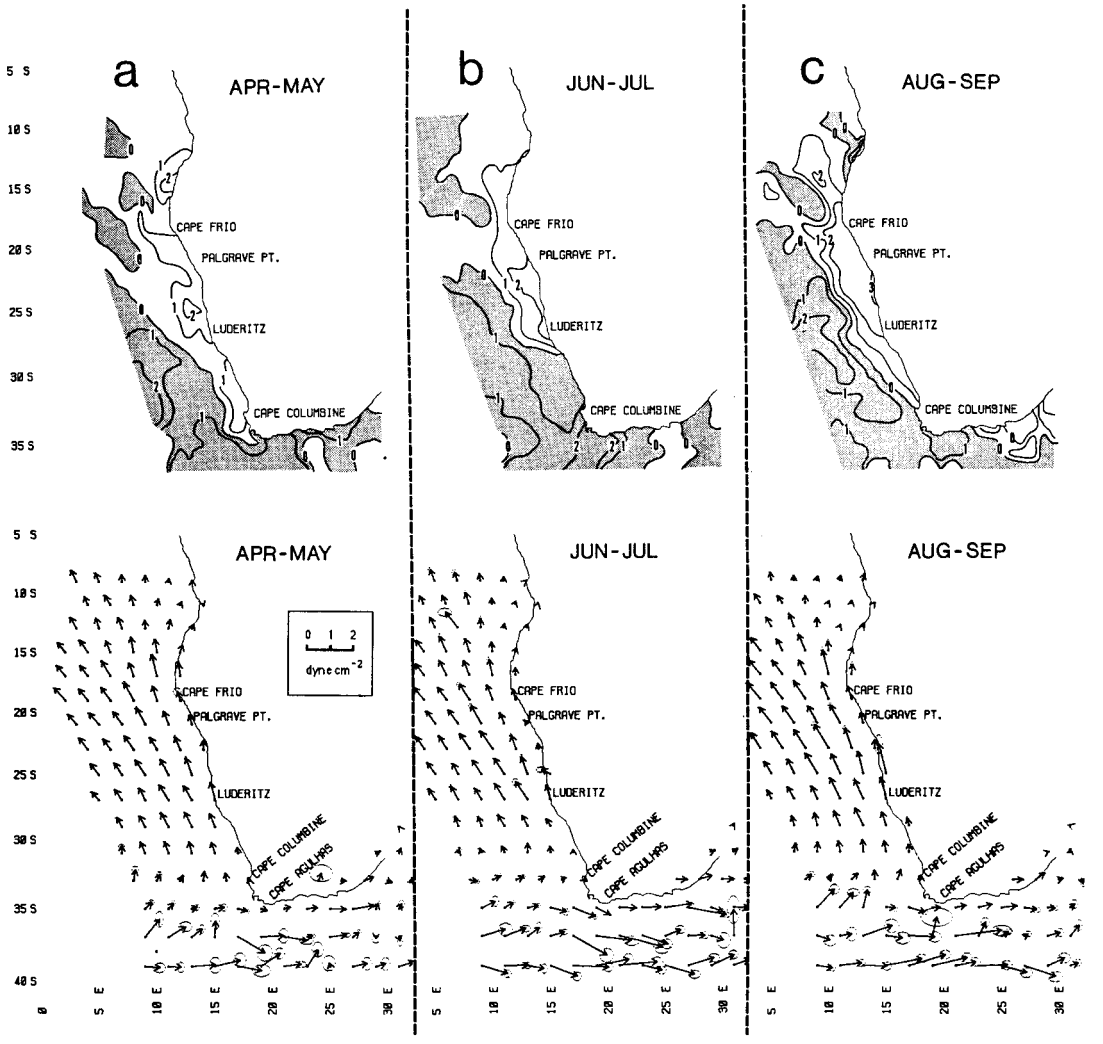

FIG. 9. Benguela Current region: wind-stress curl (10^{-8} dyn cm^{-3}) and surface wind-stress (dyn cm^{-2}) distributions. Contour interval is 1×10^{-8} dyn cm^{-3} and regions of anticyclonic curl are shaded. Wind-stress vectors are plotted at alternate latitude and longitude intersections, and symbols are scaled according to the key on the chart. (a) April–May, (b) June–July, (c) August–September,

relatively easy to recognize major errors of this type and to ensure that they were effectively removed by the smoothing and were not reinserted.

The entire process was applied independently to each 2-month sample set. No conscious transfer of information between sample sets was allowed. The six maps presented in each of Figs. 7–10 are thus based as independently from one another as possible, in spite of the subjective aspects of their construction. No "after the fact" recontouring has been performed to bring indicated features into better conformity among different maps, even when after reexamination, the data might have supported it.

To aid interpretation of the wind-stress curl distributions (Figs. 7–10), we have juxtaposed corresponding distributions of wind-stress vector symbols. Vectors are shown only at alternate grid points in both latitude and longitude to avoid clutter. Thus, the wind-stress vector maps represent only one-fourth of the total number of $1° \times 1°$ areal samples which have been incorporated in each corresponding wind-stress curl map. No smoothing has been employed in the vector

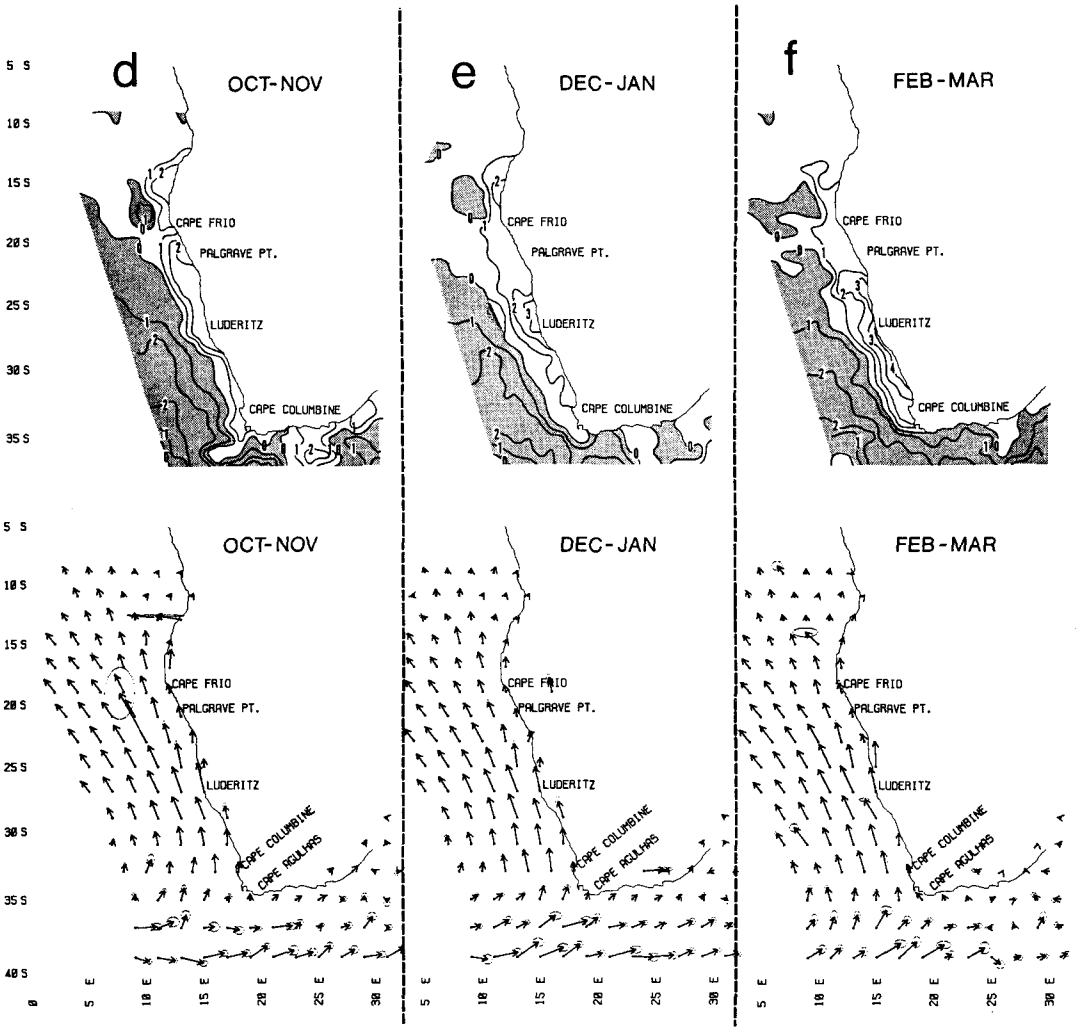

FIG. 9. (*Continued*) (d) October–November, (e) December–January, and (f) February–March.

presentations. Each vector represents a dataset that is entirely independent of any data reflected in any of the other vectors in any of the maps. The degree of coherence among the vectors in these maps provides a visual gauge to the internal consistency among independent $1° \times 1°$ bimonthly datasets. To indicate the relative effects of sampling errors versus real small-scale differences, error ellipses, having axes defined by the standard errors of the two component means defining each vector, are outlined by fine dots at the head of each vector symbol. These error ellipses tend to be visually apparent only when the standard errors are rather large and are more obvious in the data-poor regions (e.g., Fig. 10) than in the regions where data are abundant (Figs. 7 and 8).

d. Significance of the curl features

Summaries of standard errors of the curl estimates (e.g., Fig. 5) indicate that the mode of the distribution of standard errors will lie near 1×10^{-8} dyn cm^{-3} (i.e., one contour interval in Figs. 7–10) for data densities of the order of 200–300 observations per one-degree square. For one contour interval to generally correspond to about two standard error units, it would require on the order of 1000 observations per one-degree

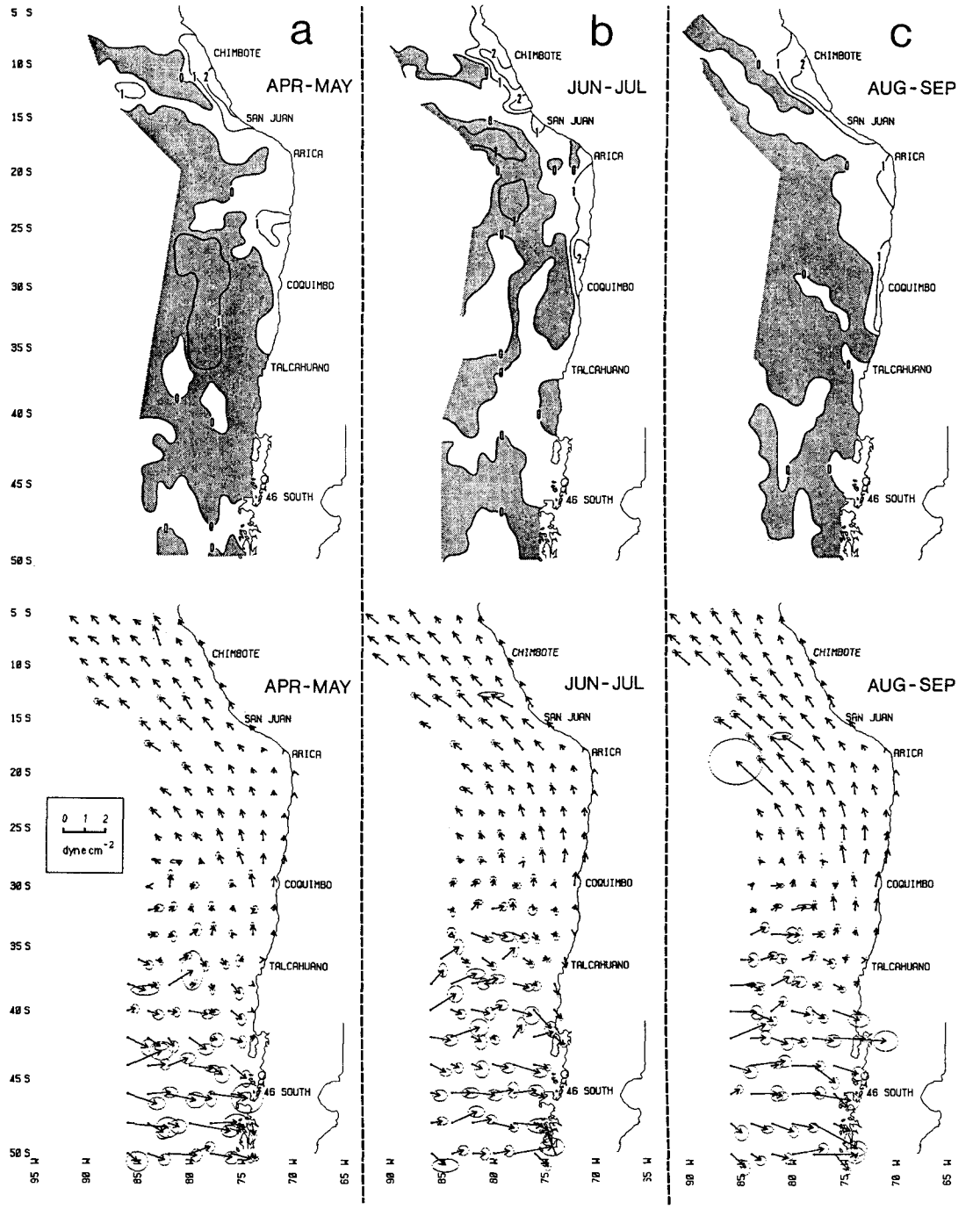

FIG. 10. Peru/Humboldt Current region: wind-stress curl (10^{-8} dyn cm^{-3}) and surface wind-stress (dyn cm^{-2}) distributions. Contour interval is 1×10^{-8} dyn cm^{-3} and regions of anticyclonic curl are shaded. Wind-stress vectors are plotted at alternate latitude and longitude intersections, and symbols are scaled according to the key on the chart. (a) April–May, (b) June–July, (c) August–September,

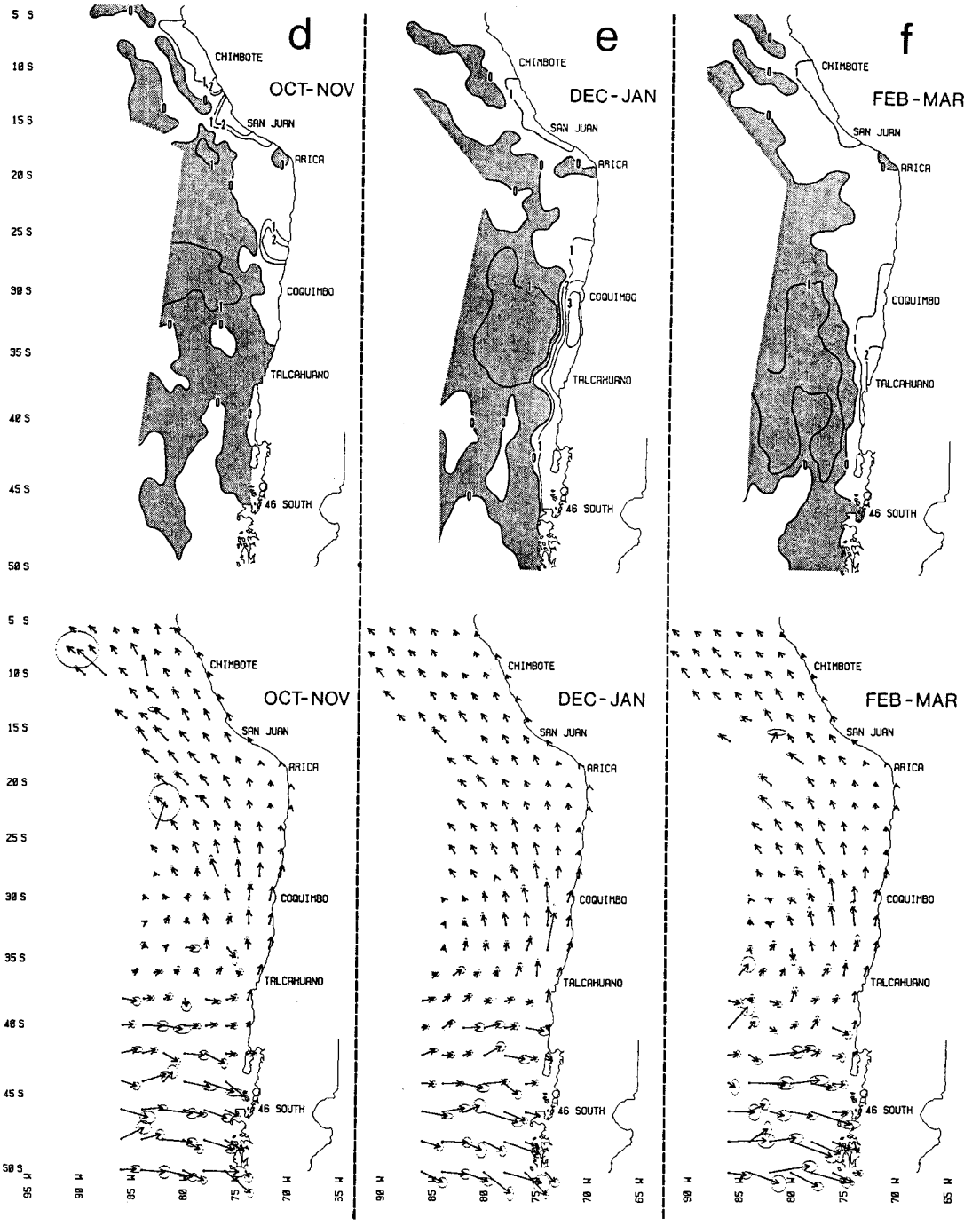

FIG. 10. (*Continued*) (d) October–November, (e) December–January, and (f) February–March.

square. In the process used to construct the fields, a large proportion of highly significant estimates allows quite a fine scale of detail (~1° to 2° scale) to be reinserted into the smoothed distributions, even after the discard of estimates either carrying large standard errors or lacking consistency between adjacent one-month subsamples.

Reference to Fig. 3 indicates high frequencies of significant curl estimates on the 1° scale might be expected in areas roughly corresponding to shaded areas of Figs. 3a, 3b, and 3d. (Recall that the data densities shown in Fig. 3 should be reduced by a factor of approximately 1/12 to reflect the density of data actually used in the curl estimates for each 2-month seasonal segment in those three regions.)

For example, the curl features shown off the Iberian Peninsula (Fig. 8) during spring and summer are judged to be highly significant on small scales (approaching 1°), both because of the extremely high data densities in that region and because multiple contours define rather small-scale features. Likewise, intense curl features near the coast along northwest Africa, south of Cabo Bojador, are likewise expected to be highly significant. However, those features to the north of Cabo Bojador are more questionable, particularly near the coast. In the California Current region (Fig. 7), the intense wind-stress curl indicated for the Southern California Bight likewise appears to be highly significant on small scales. Along the coast of Baja California one also finds adequate numbers of observations, but few features are strongly defined (i.e., by more than a single contour interval).

In other regions with lower data densities, our distributions lack significant features on such small scales. This results because the lack of highly stable features (i.e., carrying small standard errors in the 1° estimates and consistency among independent 1-month subsamples) has prevented small-scale details from being reinserted into the objectively smoothed distributions by the subjective analysis process. In some extremely data-poor regions offshore of Chile there are large areas where the characteristic one-degree sample size is only on the order of 10 to 20 observations per 1° square per 2-month seasonal segment. In these cases, the filtered distributions were too noisy to be effectively contoured, even on the 3° × 3° scale, and contours had to be drawn very roughly through large areas of ocean (in some cases on the 5° to 10° scale). Obviously, detailed locations of single contours that are not associated with nearby contours (i.e., that reflect less than one contour interval of gradient) are not to be taken very seriously in any of the areas and certainly not in data-poor regions, such as off western South America.

In attempting to merge information that may be significant on different scales in different parts of the distributions into a single description, we recognize certain problems in conveniently judging significance. The only scales that are consistently supported by sufficient data in all of the areas treated are the rather large (~10°) scales for which descriptions have already been made available (e.g., Hellerman and Rosenstein 1983). However, real, significant features supported by real data on much smaller scales exist that undoubtedly have important dynamical and ecological consequences in these eastern boundary current regions. We have done our best to "squeeze out" the smallest data-supported scales at every location while being conservative. Our purpose has been to avoid depicting features of quite questionable validity. Therefore, a lack of fine-scale wind-stress curl features in certain parts of the distributions does not mean that no such detail exists, but that we cannot confidently assert that it does.

We believe that the easiest and most useful gauge of significance of the features shown in Figs. 7–10 is the consistency exhibited among the independent distributions for different 2-month segments of the annual cycle. As described above, care has been taken to avoid transferring any information between such segments (i.e., we have consciously avoided interpretive contouring of the data in light of previously contoured distributions for the same area). Thus, when a feature exhibits consistency or regular seasonal progression through a portion of the annual cycle (i.e., between independent adjacent 2-month segments), we suggest that the reader consider it as being a real characteristic feature of the actual long-term mean wind-stress curl field. When any feature appears in only one of the distributions, without reasonable corroboration in the adjacent 2-month seasonal segments, it should be ignored. Indeed, this is the point of view taken in the descriptions that follow.

3. Results

a. The California Current region

Anticyclonic wind-stress curl, associated with the generally equatorward wind flow within the eastern leg of the North Pacific subtropical anticyclone, dominates the offshore portions of the California Current region (Fig. 7). Adjacent to the coast, the wind-stress curl tends to be cyclonic. Thus, Ekman divergence dominates at the ocean surface near the coast, and Ekman convergence is dominant in the offshore region.

The transition zone between the regions of cyclonic and anticyclonic curl is associated with an offshore maximum in the alongshore wind stress. This contour of zero curl lies approximately 200 to 300 km offshore and parallels the coastline along the entire eastern boundary between northern Baja California and Vancouver Island, from April through September (Figs. 7d, 7e, and 7f). The cross-shore profile of alongshore stress shows a decrease in magnitude on either side of the maximum. This structure, which is very characteristic of these climatological distributions, was previously noted by Munk (1950), Yoshida and Mao

(1957), Reid et al. (1958), and Nelson (1977). Moreover, the strong tendency for the alongshore wind stress to increase with distance from the coast (and for the nearshore coastal upwelling regime to be influenced by cyclonic wind-stress curl) is also evident from more recent observational studies off the coasts of Oregon and central California, as described by Halpern (1976), Beardsley et al. (1987), and Huyer and Kosro (1987).

A local maximum of cyclonic curl is associated with the Southern California Bight throughout the year. During fall and winter (Figs. 7a and 7b) substantial cyclonic curl extends northward along the coast from the Southern California Bight, nearly reaching Cape Mendocino. In late winter and spring (Figs. 7c and 7d) a second local maximum extends south from Cape Mendocino to include the area off San Francisco and Monterey Bay. By early summer, when the seasonal coastal upwelling regime has extended northward to influence essentially the entire west coast of the United States (Bakun et al. 1974), strong cyclonic curl is the rule along nearly the entire coastline of the region (Fig. 7e). In late summer, the strongest wind-stress curl in the region tends to be located adjacent to Cape Mendocino (Fig. 7f).

Throughout the year there is a consistent tendency for a lobe of anticyclonic curl to penetrate coastward from the offshore region to contact the coast of Baja California in the vicinity of Punta Baja, separating cyclonic curl regions to the north and south. Punta Baja is the site of the local maximum in coastal upwelling (Bakun and Nelson 1977). In this area, maximum equatorward alongshore wind stress occurs at the coast. This particular anticyclonic curl feature is an exception to the general pattern noted elsewhere in the region (and also in the other regions shown in Figs. 8, 9, and 10) of cyclonic curl extending some hundreds of kilometers seaward of coastal upwelling regimes.

Diagonal hatching in the area off the coast of the Pacific Northwest, shown in Fig. 7, is inserted to indicate an apparent tendency for anticyclonic wind-stress curl to exist very near the coast. The unsmoothed monthly distributions in this region have a particularly noisy appearance, with indications of generally cyclonic curl being interrupted by intense bull's-eyes of anticyclonic curl, which are generally confined to a single grid point and are characterized by large standard errors. When the averaging period is expanded, these bull's-eyes tend to coalesce, so that in the composite annual mean the area directly adjacent to the coast is predominantly occupied by anticyclonic wind-stress curl. On the scale of these computations, the situation very near the coasts of Oregon and Washington appears to be a variable mixture of more persistent weak cyclonic curl (perhaps related to lateral boundary layer effects in situations where winds are directed equatorward), broken intermittently by more intense episodes of anticyclonic curl (perhaps related to poleward winds associated with storm events). Higher resolution (0.2° × 0.2° grid) distributions of wind stress (unpublished data) for this portion of the coast show certain indications of a characteristic maximum of equatorward wind stress within about 10 km of the coast.

One of the purposes of the present study was to check for suspected scale-related artifacts in Nelson's (1977) wind stress and wind-stress curl distributions, which have been widely used in diagnosing the dynamics of the California Current System. In general, the offshore scale of major wind-stress curl features exhibited in the smaller-scale "staggered grid" curl estimates (Fig. 7) is consistent with Nelson's earlier work. However, certain local instances of offshore "bowing" of curl contours seaward of coastal indentations seen in Nelson's maps are much attenuated in these revised distributions (Fig. 7). Apparently these bowed features are scale-related artifacts, where the strong curl due to "wind shadow" in the coastal indentations propagates seaward due to the scale of the computation. Thus, the staggered grid technique (Fig. 1b) appears to provide a substantial improvement over the more standard finite difference method near boundary features, where a quite abrupt small-scale pattern exists. One additional advantage of the staggered grid technique is that only directly adjacent curl estimates share data. This makes it easier to subjectively recognize, or to objectively filter, alternating intense spikes of positive and negative curl, which are indicative of "data problems" in the particular shared gridpoint sample (see section 2c).

b. The Canary Current region

North of about 15°N, the Canary Current region (Fig. 8) exhibits a similar general dominance of anticyclonic wind-stress curl offshore and cyclonic curl adjacent to the coast. This characteristic pattern conforms to Mittelstaedt's (1983) description of seasonal variations of winds and surface circulation off northwest Africa. Near 15°N, the anticyclonic curl tends to be truncated by a zonal band of cyclonic curl that extends seaward to beyond the area treated in this study. During fall (Fig. 8a) cyclonic curl maxima are located in coastal bights off Ifni and between Cap Blanc and Cap Vert. As the seasons progress, the maxima shift to positions more directly associated with major capes. Particularly strong cyclonic curl lies directly adjacent to Cap Sim during spring and summer (Figs. 8d and 8e), the seasons of vigorous coastal upwelling (Wooster et al. 1976). Near the coast of the Iberian Peninsula, the mean curl distribution is rather weak and irregular during fall and early winter, but becomes strongly cyclonic during spring and summer, when spatially separated wind-stress curl maxima appear adjacent to the northwestern coast of the Iberian Peninsula and off southern Portugal. Although cyclonic curl near the coastal boundary appears to be the general rule, McClain et al. (1980) observed strong anticyclonic curl adjacent to the coast at Cape Finisterre, Spain, which

they related to channeling of winds along the axes of the rias (inlets), located on the northwest coast of Spain. Such features appear to be intermittent and narrowly confined to the coast and, therefore, cannot be resolved by these methods.

A lobe of anticyclonic wind-stress curl extends to the coast near Cabo Bojador during fall and winter (Figs. 8a, 8b, and 8c). The position of this lobe relative to the equatorward wind flow in the subtropical anticyclone is fairly similar to that of the persistent lobe of anticyclonic curl off Punta Baja in the California Current region. However, the lobe off Cabo Bojador and a similar lobe north of Cap Sim do not exhibit the same degree of persistence through the spring and summer upwelling seasons. In fact, the areas off Cap Sim and Cabo Bojador tend to be sites of strong cyclonic curl in the spring through late summer (Figs. 8d, 8e, and 8f). Moreover, a lobe of anticyclonic wind-stress curl, rather than being associated with any coastal protuberance, appears to extend directly into the coastal bight near Ifni during late spring and early summer.

An interesting tendency for the offshore area of anticyclonic curl to be split by a region of cyclonic (or very weak anticyclonic) curl in the region some 5° to 10° longitude offshore, from Cabo Bojador to somewhat south of Cap Blanc, appears in most of the Canary Current distributions. The area from about 10° to 20°N is characterized by cyclonic wind-stress curl during the summer months (Figs. 8e and 8f). However, during the other seasons of the year, a region of anticyclonic curl extends to the south of Cap Vert between 21° and 25°W.

c. *The Benguela Current region*

In the Benguela Current region, the coastal area of cyclonic wind-stress curl appears as a wedge extending from the vicinity of 20°S, narrowing in offshore extent toward the south. The wedge has its most limited poleward extent in austral winter (Fig. 9b) when it reaches to just south of Lüderitz. By early spring the wedge has extended to Cape Columbine (Fig. 9c) and beyond the Cape of Good Hope by late spring (Fig. 9d), where it remains until it retreats northward again with the approach of austral winter.

Equatorward of 20°S, the distributions are less distinct. A sparsity of observations in that region (Fig. 3d), and associated large sampling errors, make the computed curl distributions very noisy and somewhat uncertain. However, one very persistent feature is an area of anticyclonic curl, some hundreds of kilometers in diameter lying about 200 km offshore, and extending somewhat northward of Cape Frio. Evidence for this particular feature is found in all 12 independent monthly distributions. In the region north of 15°S, there appears to be some tendency for anticyclonic curl near the coast in late austral winter to spring. In austral summer and fall, the region within 700 km of the coast appears to be dominated by cyclonic wind-stress curl.

d. *The Peru/Humboldt Current region*

During austral fall (Fig. 10a) in the Peru/Humboldt Current region, cyclonic curl adjacent to the coast extends south to the vicinity of Talcahuano. Local curl maxima appear along the coast of Peru from the vicinity of San Juan to north of Chimbote, and off Chile at about 25°S. The maximum off Peru appears to maintain its location throughout the year, strengthening in austral winter and relaxing somewhat in summer. The wind-stress curl maximum off Chile moves poleward from winter to summer, reaching maximum intensity off the stretch of coastline from 30° to 34°S in austral summer (Fig. 10e). This maximum appears to move even farther south in late summer (Fig. 10f), to a position just north of Talcahuano, before weakening greatly and retreating back northward in fall.

There are consistent indications of anticyclonic curl within the coastal bight near Arica. This is in contrast to the consistent cyclonic curl found to characterize major coastal bights in other eastern boundary current regions, for example, in the Southern California Bight (Fig. 7) and between Cap Blanc and Cap Vert (Fig. 8). This is probably due to the fact that the coastal shape here is such that the equatorward wind, which flows along the Chilean coast, blows uninterruptedly into the bight, rather than being deflected by a major change in coastline orientation at the upwind edge of the bight.

A persistent, elongated lobe of anticyclonic curl exists off northern Peru. This feature is definitely separated from the general anticyclonic curl in the offshore region to the south. In view of the low data density available for the region, the consistency of this lobe in location and general shape among these independently prepared distributions is remarkable. The lobe appears to be aligned along the axis of the trade wind flow, which veers westward away from the coast in that area.

4. Generalizations

Eastern boundary current regions are characterized by anticyclonic wind-stress curl in the offshore portions. Near the coastal boundary, the wind-stress curl tends to be cyclonic, particularly during the coastal upwelling seasons (i.e., seasons in which the average wind stress is directed alongshore and equatorward). These cyclonic curl areas typically extend 200 to 300 km offshore. Thus, the coastal upwelling that occurs within several tens of kilometers of the coast is typically augmented by upward Ekman pumping (oceanic upwelling) over a much larger offshore extent. The coastal cyclonic curl regions tend to have their greatest alongshore extents during the summer seasons in the respective hemispheres.

Particularly intense cyclonic wind-stress curl is found adjacent to capes during summer coastal upwelling maxima. During seasons of strong equatorward, alongshore wind stress, the offshore profile of stress bears at least a qualitative resemblance to a lateral frictional boundary layer, characterized by an offshore maximum in wind velocity and a decay of velocity toward the coast. Coastal protuberances would tend to narrow the layer locally, leading to intensified cyclonic curl.

The alongshore jet structure of the low-level winds off the western United States has been modeled by Chao (1985) as a boundary layer response of the large-scale zonal westerlies to blocking by the coastal mountain ranges along the west coast of North America. Chao also indicates that thermal forcing by the land–ocean temperature contrast could reinforce the jet structure during the summer and, thereby, account for the observed intensification of alongshore wind near the coast during the summer season.

During fall and winter when the upwelling system weakens, the most intense cyclonic curl is associated with coastal bights. During winter, the regime tends to be intermittently broken by the passage of cyclonic storms, which often involve intense winds having poleward and onshore components. Although maritime data cannot define synoptic situations on these small spatial scales, it would seem reasonable that such winds might tend to reach maximum velocities as they are narrowed and deflected toward a more alongshore direction, directly adjacent to the barrier presented by the coastal boundary. Such effects might tend to be strongest where the wind flow was directed into coastal bights, leading to the tendency during winter for cyclonic curl maxima to lie within such concave coastal segments.

In various locations, such as at Punta Baja in the California Current region, near Cabo Bojador and Cap Sim in the Canary Current region, slightly to the north and offshore of Cape Frio in the Benguela Current region, and offshore of Chimbote in the Peru/Humboldt region, distinctive lobes, or isolated patches of anticyclonic curl, appear either in contact with, or within several hundred kilometers of, the coastal boundary. These appear typically to be located in areas where the equatorward wind flow begins to veer offshore to merge into the tropical trade-wind circulation.

Acknowledgments. We thank Drs. Robert L. Smith and Adriana Huyer for many fruitful discussions on eastern boundary current systems, and Dr. Mary L. Batteen for review of the manuscript. Comments by two anonymous reviewers have been very helpful. Mr. Art Stroud, of Compass Systems, Inc., aided in data processing and mapping of the distributions. Access to surface marine data archives and computer resources was provided by the U.S. Navy, Fleet Numerical Oceanography Center, Monterey, California. This work was sponsored in part by the Naval Postgraduate School and the Office of Naval Research's Ocean Science Directorate.

REFERENCES

Abbott, M. R., and P. M. Zion, 1987: Spatial and temporal variability of phytoplankton pigment off northern California during Coastal Ocean Dynamics Experiment 1. *J. Geophys. Res.*, **92,** 1745–1755.

Bakun, A., 1978: Guinea Current upwelling. *Nature,* **271,** 147–150.

——, 1990: Global climate change and intensification of coastal ocean upwelling. *Science,* **247,** 198–201.

——, and C. S. Nelson, 1977: Climatology of upwelling related processes off Baja California. California Cooperative Oceanic Fisheries Investigations Reports, 19, 107–127.

——, and R. H. Parrish, 1990: Comparative studies of coastal pelagic fish reproductive habitats: The Brazilian sardine (*Sardinella aurita*). *J. Cons. Int. Explor. Mer.*, **46,** 269–283.

——, D. R. McLain and F. V. Mayo, 1974: The mean annual cycle of coastal upwelling off western North America as observed from surface measurements. *Fish. Bull.*, **72,** 843–844.

Beardsley, R. C., C. E. Dorman, C. A. Friehe, L. K. Rosenfeld and C. D. Winant, 1987: Local atmospheric forcing during the Coastal Ocean Dynamics Experiment, 1. A description of the marine boundary layer and atmospheric conditions over a northern California upwelling region. *J. Geophys. Res.*, **92,** 1467–1488.

Beaton, A. E., and J. W. Tukey, 1974: The fitting of power series, meaning polynomials, illustrated on band-spectroscopic data. *Technometrics,* **16,** 147–185.

Beers, Y., 1953: *Introduction to the Theory of Error.* Addison-Wesley, 65 pp.

Blanc, T. V., 1985: Variation of bulk-derived surface flux, stability, and roughness results due to the use of different transfer coefficient schemes. *J. Phys. Oceanogr.*, **15,** 650–669.

Böning, C. W., R. Döscher and H.-J. Isemer, 1991: Monthly mean wind stress and Sverdrup transports in the North Atlantic: A comparison of the Hellerman-Rosenstein and Isemer-Hasse climatologies. *J. Phys. Oceanogr.*, **21,** 221–235.

Breidenbach, J., 1990: EOFs of pseudostress over the Indian Ocean (1977–85). *Bull. Amer. Meteor. Soc.*, **71,** 1448–1454.

Brink, K. H., D. C. Chapman and G. R. Halliwell, Jr., 1987: A stochastic model for wind-driven currents over the continental shelf. *J. Geophys. Res.*, **92,** 1783–1797.

Cardone, V. J., J. G. Greenwood and M. A. Cane, 1990: On trends in historical marine wind data. *J. Climate,* **3,** 113–127.

Carton, J. A., and S. G. H. Philander, 1984: Coastal upwelling viewed as a stochastic phenomenon. *J. Phys. Oceanogr.*, **14,** 1499–1509.

Chao, S.-Y., 1985: Coastal jets in the lower atmosphere. *J. Phys. Oceanogr.*, **15,** 361–371.

Chelton, D. B., 1980: Low frequency sea level variability along the west coast of North America. Ph.D. dissertation, University of California, San Diego, 212 pp.

——, 1982: Large-scale response of the California Current to forcing by the wind-stress curl. California Cooperative Oceanic Fisheries Investigations Reports, 23, 130–148.

Cleveland, W. S., 1981: LOWESS: A program for smoothing scatterplots by robust locally weighted regression. *Amer. Statist.*, **35,** p. 54.

Cummins, P. F., L. A. Mysak and K. Hamilton, 1986: Generation of annual Rossby waves in the North Pacific by the wind-stress curl. *J. Phys. Oceanogr.*, **16,** 1179–1189.

Düing, W., F. Ostapoff and J. Merle, 1980: *Physical Oceanography of the Tropical Atlantic during GATE.* University of Miami, 117 pp.

Evenson, A. J., and G. Veronis, 1975: Continuous representation of wind stress and wind-stress curl over the world ocean. *J. Mar. Res.*, **33**(Suppl.), 131–144.

Goldenberg, S. B., and J. J. O'Brien, 1981: Time and space variability of tropical Pacific wind stress. *Mon. Wea. Rev.*, **109,** 1190–1207.

Halpern, D., 1976: Measurements of near-surface wind stress over an upwelling region near the Oregon coast. *J. Phys. Oceanogr.*, **6,** 108–112.

Hastenrath, S., and P. J. Lamb, 1977: *Climatic Atlas of the Tropical Atlantic and Eastern Pacific Oceans.* University of Wisconsin Press, 15 pp., 97 figs.

Hellerman, S., and M. Rosenstein, 1983: Normal monthly wind stress over the world ocean with error estimates. *J. Phys. Oceanogr.*, **13,** 1093–1104.

Hickey, B. M., 1979: The California Current System—hypotheses and facts. *Progress in Oceanography,* Vol. 8, Pergamon, 191–279.

Hsiung, J. 1986: Mean surface energy fluxes over the global ocean. *J. Geophys. Res.*, **91,** 10 585–10 606.

Hurlburt, H. E., and J. D. Thompson, 1973: Coastal upwelling on a β-plane. *J. Phys. Oceanogr.*, **3,** 16–32.

Huyer, A., and P. M. Kosro, 1987: Mesoscale surveys over the shelf and slope in the upwelling region near Point Arena, California. *J. Geophys. Res.*, **92,** 1655–1681.

Isemer, H.-J., and L. Hasse, 1991: The scientific Beaufort equivalent scale: Effects on wind statistics and climatological air–sea flux estimates in the North Atlantic Ocean. *J. Climate,* **4,** 819–836.

Large, W. G., and S. Pond, 1981: Open ocean momentum flux measurements over the ocean. *J. Phys. Oceanogr.*, **11,** 324–336.

McClain, C. R., S.-Y. Chao, L. P. Atkinson, J. O. Blanton and F. de Castillejo, 1986: Wind-driven upwelling in the vicinity of Cape Finisterre, Spain. *J. Geophys. Res.*, **91,** 8470–8486.

McCreary, J. P., Jr., P. K. Kundu and S.-Y. Chao, 1987: On the dynamics of the California Current system. *J. Mar. Res.*, **45,** 1–32.

Mittelstaedt, E., 1983: The upwelling area off northwest Africa—a description of phenomena related to coastal upwelling. *Progress in Oceanography,* Vol. 12, Pergamon, 307–331.

Munk, W. H., 1950: On the wind-driven ocean circulation. *J. Meteor.*, **7,** 79–93.

Nelson, C. S., 1977: Wind stress and wind-stress curl over the California Current. NOAA Tech. Rep. NMFS SSRF-714, U.S. Dept. of Commerce, 87 pp.

Parrish, R. H., A. Bakun, D. M. Husby and C. S. Nelson, 1983: Comparative climatology of selected environmental processes in relation to eastern boundary current pelagic fish reproduction. *Proc. of the Expert Consultation to Examine Changes in Abundance and Species Composition of Neritic Fish Resources,* G. D. Sharp and J. Csirke, Eds., *FAO Fish. Rep.*, San Jose, Costa Rica, FAO, 291, 731–778.

Pedlosky, J., 1974: Longshore currents, upwelling, and bottom topography. *J. Phys. Oceanogr.*, **4,** 214–226.

Peláez, J., and J. A. McGowan, 1986: Phytoplankton pigment patterns in the California Current as determined by satellite. *Limnol. Oceanogr.*, **31,** 927–950.

Perigaud, C., P. Delecluse and J. F. Minster, 1989: Wind stress over the Arabian Sea from ship reports and Seasat scatterometer data. *Mon. Wea. Rev.*, **117,** 2348–2364.

Rabiner, L. R., M. R. Sambur and C. E. Schmidt, 1975: Applications of a nonlinear smoothing algorithm to speech processing. *IEEE Trans. Acoust., Speech Signal Proc.*, **ASSP-23,** 552–557.

Ramage, C. S., 1987: Secular change in reported surface wind speeds over the oceans. *J. Climate Appl. Meteor.*, **26,** 525–528.

Reid, J. L., Jr., G. I. Roden and J. G. Wyllie, 1958: Studies of the California Current system. California Cooperative Oceanic Fisheries Investigations Reports, **6,** 28–56.

Rienecker, M. M., and L. L. Ehret, 1988: Wind-stress curl variability over the North Pacific from the Comprehensive Ocean–Atmosphere Data Set. *J. Geophys. Res.*, **93,** 5069–5077.

——, C. N. K. Mooers and A. R. Robinson, 1987: Dynamical interpolation and forecast of the evolution of mesoscale features off northern California. *J. Phys. Oceanogr.*, **17,** 1189–1213.

Roden, G. I., 1972: Large-scale upwelling off northwestern Mexico. *J. Phys. Oceanogr.*, **2,** 184–189.

Saunders, P. M., 1976: On the uncertainty of wind-stress curl calculations. *J. Mar. Res.*, **34,** 155–160.

Servain, J., and D. M. Legler, 1986: Empirical orthogonal function analysis of tropical Atlantic sea surface temperature and wind stress. *J. Geophys. Res.*, **91,** 14 181–14 191.

Shearman, R. J., 1983: The Meteorological Office main data bank. *Meteor. Mag.*, **112,** 1–10.

Smith, R. L., 1968: Upwelling. *Oceanogr. Mar. Biol. Ann. Rev.*, **6,** 11–46.

Smith, S. D., 1988: Coefficients for sea surface wind stress, heat flux, and wind profiles as a function of wind speed and temperature. *J. Geophys. Res.*, **93,** 15 467–15 472.

Trenberth, K. E., W. G. Large and J. G. Olson, 1989: The effective drag coefficient for evaluating wind stress over the oceans. *J. Climate,* **2,** 1507–1516.

Weare, B. C., 1989: Uncertainties in estimates of surface heat fluxes derived from marine reports over the tropical and subtropical oceans. *Tellus,* **41A,** 357–370.

White, W. B., 1985: The resonant response of interannual baroclinic Rossby waves to wind forcing in the eastern midlatitude North Pacific. *J. Phys. Oceanogr.*, **15,** 403–415.

Willebrand, J., 1978: Temporal and spatial scales of the wind field over the North Pacific and North Atlantic. *J. Phys. Oceanogr.*, **8,** 1080–1094.

Wooster, W. S., and J. L. Reid, Jr., 1963: Eastern boundary currents. *The Sea,* Vol. 2, M. N. Hill, Ed., Wiley Interscience, 253–280.

——, A. Bakun and D. R. McLain, 1976: The seasonal upwelling cycle along the eastern boundary of the North Atlantic. *J. Mar. Res.*, **34,** 131–141.

Wyrtki, K., and G. Meyers, 1976: The trade wind field over the Pacific Ocean. *J. Appl. Meteor.*, **15,** 698–704.

Yoshida, K., 1955a: Coastal upwelling off the California coast. *Rec. Oceanogr. Works Japan,* **2,** 8–20.

——, 1955b: An example of variations in oceanic circulation in response to the variations in wind field. *J. Oceanogr. Soc. Japan.*, **11,** 103–108.

——, and H.-L. Mao, 1957: A theory of upwelling of large horizontal extent. *J. Mar. Res.*, **16,** 40–54.